This paper describes objective technical results and analysis. Any subjective views or opinions that might be expressed in the paper do not necessarily represent the views of the U.S. Department of Energy or the United States Government.

SAND2018-6781J

Detecting lightning infrasound using a high-altitude balloon

Oliver D. Lamb[1], Jonathan M. Lees[1], Daniel C. Bowman[2]

[1]Department of Geological Sciences, The University of North Carolina at Chapel Hill, Chapel Hill, North Carolina, USA
[2]Sandia National Laboratories, Albuquerque, New Mexico, USA

Key Points:

- First lightning infrasound detected using free-flying balloon at stratospheric altitudes over Tasman Sea in May 2016.
- Infrasonic signals matched with a few lightning strokes within 100 km range of balloon as it flew over at least two thunderclouds.
- Only a fraction of the expected infrasound signals were detected, and the cause of this remains unclear.

Corresponding author: Oliver Lamb, olamb@email.unc.edu

Sandia National Laboratories is a multimission laboratory managed and operated by National Technology & Engineering Solutions of Sandia, LLC, a wholly owned subsidiary of Honeywell International Inc., for the U.S. Department of Energy's National Nuclear Security Administration under contract DE-NA0003525.

Abstract

Acoustic waves with a wide range of frequencies are generated by lightning strokes during thunderstorms, including infrasonic waves (0.1 to 20 Hz). The source mechanism for these low frequency acoustic waves is still debated and studies have so far been limited to ground-based instruments. Here we report the first confirmed detection of lightning generated infrasound with acoustic instruments suspended at stratospheric altitudes using a free-flying balloon. We observe high-amplitude signals generated by lightning strokes located within 100 km of the balloon as it flew over the Tasman Sea on 17 May 2016. The signals share many characteristics with waveforms recorded previously by ground-based instruments near thunderstorms. The ability to measure lightning activity with high-altitude infrasound instruments has demonstrated the potential for using these platforms to image the full acoustic wavefield in the atmosphere. Furthermore, it validates the use of these platforms for recording and characterizing infrasonic sources located beyond the detection range of ground-based instruments.

Plain-language summary

Lightning generates sound waves across a wide range of frequencies, including below the threshold for human hearing at 20 Hz. How these waves at less than 20 Hz, also known as infrasound waves, are generated during a lightning stroke is currently an area for debate. So far, measurements of lightning infrasound waves have been limited to microphones fixed to the ground and models have shown that only a small section of sound waves actually reach the ground. Here we show lightning infrasound that has been detected using microphones suspended over a thunderstorm using a balloon flying at 32 km height. This opens up the possibility of using balloons in future studies to make better measurements of infrasound waves generated by lightning activity and in turn, give a better idea of how they are generated. It also shows how balloons can be used to record infrasound waves far away from land and therefore beyond the detection limit of ground-based microphones.

1 Introduction

Acoustic signals with frequencies between 0.02 to 20 Hz are classified as infrasound and are not audible to humans. A wide variety of sources have been found to generate infrasound, including: volcanoes, earthquakes, avalanches, tsunami, meteors, aurora, thunderstorms, wind-mountain interactions, supersonic aircraft, rockets, and chemical and nuclear explosions [*Campus and Christie*, 2010]. Infrasonic signals can travel hundreds to thousands of kilometers through the atmosphere, sampling areas from the Earth's surface up to the thermosphere. A variety of institutions maintain arrays for monitoring purposes, such as volcano observatories [*Fee and Matoza*, 2013] or the International Monitoring System [*Christie and Campus*, 2010]. The vast majority of infrasound studies currently use ground-based instrument arrays and networks. Infrasound instruments deployed on the ground may be subject to high-levels of background noise which may obscure the signals of interest, or the signals may arrive distorted due to topographic or atmospheric propagation effects [e.g. *Lacanna and Ripepe*, 2013; *Kim and Lees*, 2014]. Furthermore, the intensity of the acoustic wavefield may be as much as 50% greater directly above the source compared that at a similar horizontal distance [*Blackstock*, 2000].

A series of studies have recently taken place to explore how to fill this gap in our ability to monitor the atmospheric acoustic wavefield. These experiments have tested the use of microphones suspended underneath free-floating balloons to record infrasound at high-altitude [e.g. *Bowman and Lees*, 2015, 2017; *Bowman and Albert*, 2018]. Balloon deployments conducted as part of the NASA High-Altitude Student Platform (HASP) program described evidence of the ocean microbarom as well as other signals of unknown provenance [*Bowman and Lees*, 2015]. A follow-up experiment showed that the ocean

microbarom was often detectable in the stratosphere but not at ground-level, either due to low noise at the balloons, an elevated acoustic duct, or both [*Bowman and Lees*, 2017]. In 2017, four microphone-bearing solar balloons were launched concurrently and successfully detected and located a chemical explosion on the ground [*Bowman and Albert*, 2018]. So far, none of these experiments have confirmed the detection of other infrasonic signals from sources such as lightning storms.

Acoustic emissions from lightning, described as thunder, can produce a broadband range of frequencies. The audible component of thunder (20-20,000 Hz), as well as energy in the infrasonic range, is understood to come mostly from shock waves produced by the rapid expansion of a lightning channel due to current flow and heating [*Few et al.*, 1967]. In addition, numerous studies have observed infrasound generated by cloud-to-ground (CG) and intracloud (IC) lightning flashes [e.g. *Balachandran*, 1983; *Assink et al.*, 2008; *Farges and Blanc*, 2010; *Arechiga et al.*, 2014]. The lightning signal is often a discrete pulse characterized by an initial compression followed by a rarefaction with maximum amplitudes in the range of 0.05 to 5 Pa and a spectral peak in the range of 0.2 to 2 Hz [*Dessler*, 1973; *Bohannon et al.*, 1977; *Assink et al.*, 2008; *Campus and Christie*, 2010]. Multiple production mechanisms have been postulated for the infrasonic acoustics detected during lightning storms. This includes rapid intensification of the electric field just prior to the flash, ohmic heating of the air by charge flowing into the channel, and interaction between the positive and negative charge layers in the storm cloud [*Dessler*, 1973; *Bohannon et al.*, 1977; *Pasko*, 2009]. Furthermore, the acoustic wavefield generated by this mechanism was predicted to be orientated vertically, restricting the horizontal detection range of lightning infrasound [*Dessler*, 1973; *Pasko*, 2009]. Validation of the production mechanism and acoustic wavefield has been confounded by the difficulty in locating the charge layers in the storm cloud, as well as characterizing the structure of the parent lightning flash. Advancements in location algorithms and instruments deployments such as the Lightning Mapping Array (LMA) have produced observations that refute the previously proposed production mechanisms [*Arechiga et al.*, 2014]. Instead, the observations suggest that the infrasonic signals from lightning flashes may be produced by electrostatic interaction of charge deposited in the streamer zone of a lightning channel; that is, acoustic compression waves may be generated by electrostatic forces causing air within the streamer zone to expand [*Arechiga et al.*, 2014]. Lightning infrasound has also been detected at ranges of up to 150 km from the source, contrary to previous predictions of a vertically orientated acoustic wavefield [e.g. *Farges and Blanc*, 2010].

Here we report on detections of lightning infrasound recorded by a high-altitude balloon flying over the Tasman Sea on 17 May 2016. We present evidence for signals recorded from at least two groups of lightning flashes during a 6 hour period. Measurements suggest that the detection of lightning infrasound was limited by the distance and atmospheric conditions between source and receiver. A few example signals from lightning strokes are isolated and their waveform characteristics are briefly discussed. These observations, the first of their kind reported, suggest that microphones deployed on high-altitude balloons can offer additional insights into the production mechanisms of lightning infrasound.

2 Data

An acoustic sensor package was included as a piggyback payload on the NASA Ultra Long Duration Balloon (ULDB) flight launched from Wanaka, New Zealand on 16 May 2016. The ULDB landed in Peru on 2 July 2016 for a total flight duration of 46 days. The ULDB balloon position and height was recorded using an onboard GPS unit, and records show the full flight included a full circumnavigation of the southern hemisphere [*Bowman et al.*, 2017]. The acoustic sensor package recorded data for the first 20 days of the flight, and the ocean microbarom was recorded throughout as well as other signals of unknown provenance [*Bowman and Lees*, 2018].

The sensor package contained three InfraBSU microphones [*Marcillo et al.*, 2012]: one control and a pair with reversed polarities. The reversed polarity sensor was achieved by placing the mechanical sensor on the opposite port. The reversed polarity microphone pair were combined into a single channel via:

$$M = \frac{M_+ - M_-}{2} \tag{1}$$

where M is the data analyzed in this article, and M_+ and M_- are the data from the microphones with positive and negative polarities, respectively. The control sensor was a microphone that was disabled by removing the mechanical filter entirely. This acoustic sensor trio was designed to robustly distinguish between true pressure fluctuations and spurious signals, such as electronic interference [*Bowman et al.*, 2017]. Data was recorded at 200 samples per second at 64x gain using an Omnirecs Datacube digitizer. The microphones were not calibrated to the pressure and temperature conditions experienced during the flight, but their primary effect should be to lower the corner period of the sensors [*Bowman et al.*, 2017]. The acoustic waveforms presented here are high-pass filtered at 0.6 Hz in order to remove high-amplitude signals contributed from the ocean microbarom [*Bowman and Lees*, 2018], atmospheric gravity waves generated by thunder cloud convection [*Blanc et al.*, 2010], and balloon oscillations [*Anderson and Taback*, 1991]. (Unfiltered signals recorded by the acoustic package can be seen in Figure S1 in supplementary information.) The microphones and digitizer were each powered by separate Lithium battery packs, and contained within high density styrofoam shipping boxes for thermal insulation. Internal temperatures within the digitizer ranged from -26 to 7 °C during the flight.

The lightning stroke detections and location data used in this article were detected and recorded by the World Wide Lightning Location Network (WWLLN). The WWLLN is an instrument network capable of locating and timing lightning strokes at long range (thousands of kilometers) to within <10 km and <10 μs [*Hutchins et al.*, 2012]. The network uses very-low-frequency radio wave (3-30 kHz) receivers distributed around the globe to identify the time of group arrival for individual lightning waveforms, or sferics. The network is capable of detecting both CG and IC discharges, but the latter are typically underrepresented in detection databases as they produce weaker electromagnetic pulses [*Behnke and McNutt*, 2014]. As of 2010, the estimated detection efficiency for the network was ∼11% for all strokes and >30% for more powerful strokes [*Hutchins et al.*, 2012]. These values may seem low, but the WWLLN was not designed to detect all lightning strokes but instead to provide a global overview of lightning activity [*Dowden et al.*, 2008]. Other lightning stroke datasets may exist from other global detection networks, but were not available for the analysis presented herein.

3 Observations

The ULDB was launched from Wanaka, New Zealand just before 0000 UTC on 17 May 2016 started flying east as it ascended. Once the craft approached and breached 30 km altitude, it turned to the west and flew out over the Tasman Sea and towards Australia (Fig. 1). During this period, the WWLLN detected intense lightning activity from multiple thunderstorms approaching New Zealand from the west (Fig. 1, Movie S1 in supporting information). From 0800 to 1400 UTC, 2994 strokes were detected and located by the WWLLN across the Tasman Sea, of which 2554 were located within 500 km of the ULDB (Fig. 2a). At approximately 0945 and 1200 UTC the ULDB passed directly over or near lightning activity which correlates with an increase in acoustic activity recorded at the ULDB (Fig. 2a, b). Acoustic signals are recorded with peak-to-peak amplitudes of up to 0.05 Pa and a broadband range of frequencies from 0.6 to 20 Hz (Fig. 2b, c).

As the acoustic sensor package on the ULDB was fundamentally a single element station, back-azimuths and slowness vectors cannot be calculated to locate sources of de-

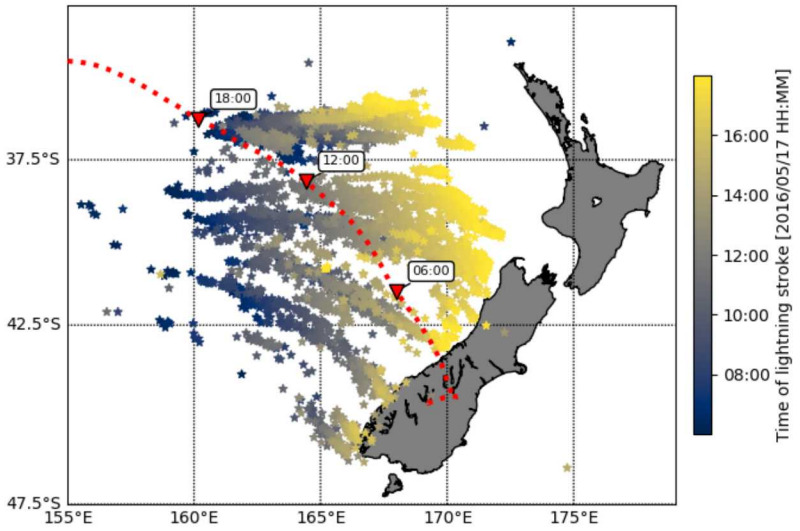

Figure 1. Map of the Tasman Sea with the locations of lightning detected by the WWLLN from 0600 to 1800 UTC on 17 May 2016, where color represents the progression of time (see colorbar). Also plotted is the path of the ULDB balloon after it was launched from Wanaka, New Zealand (red dotted line), and it's location at 0600, 1200 and 1800 UTC on 17 May 2016 (red triangles). (For an animated version of this figure, see Movie S1 in supporting information.)

tected signals. To estimate detection ranges, ray tracing was used to model infrasonic propagation paths between lightning and the ULDB. Ray tracing was performed using classical geometric acoustics techniques and a plane wave assumption, calculated within the open source GeoAc ray tracing software [*Blom and Waxler*, 2012]. Rays were launched at intervals of 1° from a point source at a height of 4 km. This source height was based on previously used heights for modeling lightning infrasound [*Pasko*, 2009; *Farges and Blanc*, 2010]. Atmospheric profiles were derived from the 12z Global Forecast System (GFS) analysis model run, located at the latitude/longitude coordinates for the ULDB at 1200 UTC on 17 May 2016 (Fig. S2 in supplementary information). For a source at 4 km height and a receiver at 32 km height, direct arrivals from the source should only be expected <110 km horizontal distance in all directions (Fig. 3). At this distance, 34 lightning strokes were recorded when the ULDB flew near a storm at approximately 1200 UTC (Fig. 4a). 10 strokes were recorded within 100 km during the earlier storm at 0945 UTC (Fig. S3 in supplementary information).

To match infrasonic signal peaks and specific lightning strokes, we compute the time needed for waveforms from each stroke within a limited distance to arrive at the ULDB. We take a simplified approach and assume that the atmosphere can be approximated with a bulk acoustic wave speed of 300 ms^{-1}. Furthermore, all acoustic waveforms arriving at the ULDB platform are assumed to be direct arrivals from the source. Out of 34 lightning strokes within 100 km of the balloon between 1130 and 1230 UTC, multiple events appear to match directly with peaks in recorded acoustic amplitudes (Fig. 4b). Here we present three matches which occur at 1145, 1148, and 1152 UTC (Fig. 4c, d, and e). Other possible matches occur at 1143, 1156 and 1205 UTC but source-signal pairs cannot be distinguished due to multiple closely spaced source strokes or infrasonic ar-

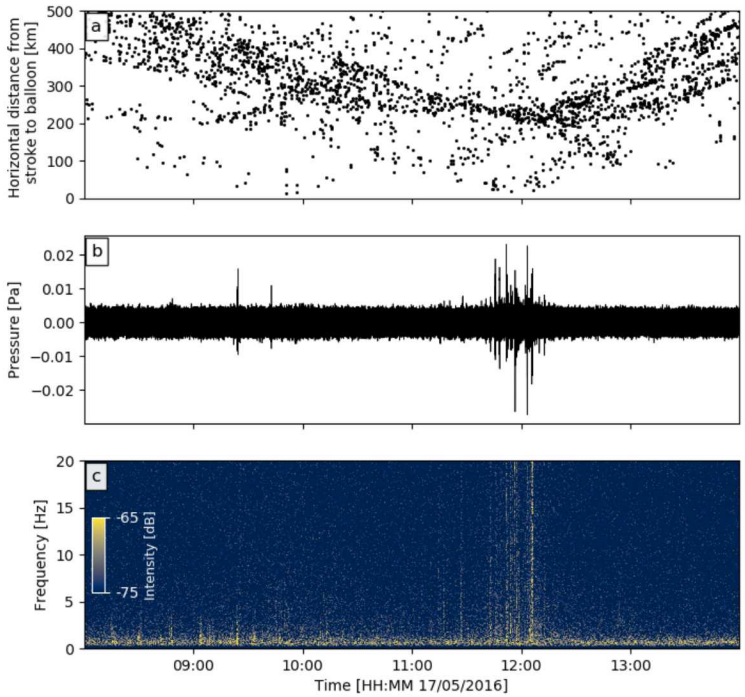

Figure 2. (a) Horizontal distances for each stroke within 500 km of the balloon's location at the time of the stroke, from 0800 to 1400 UTC on 17 May 2016. (b) High-pass filtered (0.6 Hz) infrasound over the same time period as recorded at the ULDB. (c) Frequency spectrogram of the waveform plotted in (b).

rivals. None of the 10 detected strokes directly match with infrasonic signals during the earlier storm at 0945 UTC (Fig. S3 in supplementary information).

The energy density of an expanding acoustic shock wave from a lightning stroke can be estimated from the peak frequency of the recorded waveform [*Few*, 1969]. For a given acoustic waveform with peak frequency, f_p:

$$f_p = 0.63 c_0 \sqrt{P_0/E} \tag{2}$$

where c_0 is the local speed of sound (300 ms^{-1}), P_0 is the atmospheric pressure (60 kPa for a source at 4 km altitude), and E is the energy per unit length [*Few*, 1969]. For each matched waveform plotted in Fig. 4c, d and e, we find peak frequencies of 2.65, 1.27, and 5.27 Hz, respectively (Fig. S4a in supplementary info). Using equation (2) we find a positive linear relationship between the energy densities calculated from the acoustic waveforms and the energies detected for the lightning strokes by the WWLLN (Fig. S4b in supplementary info). We also find no relationship between the calculated energy densities and the stroke-balloon distance (Fig. S4c in supplementary info).

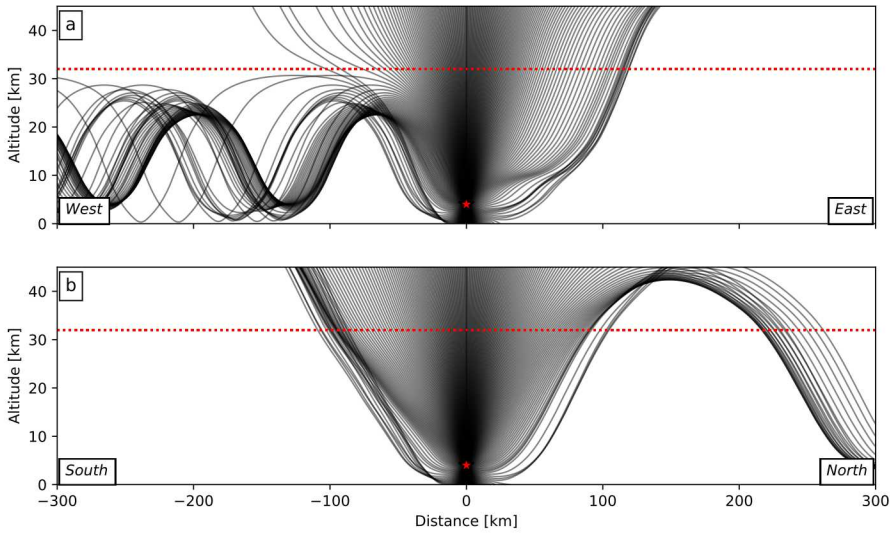

Figure 3. Ray-tracing propagation for an acoustic source (red star) at 4 km height along East-West (a) and North-South (b) profiles using realistic atmospheric conditions derived from the Global Forecast System. The red dotted line at 32 km indicates the approximate height of the ULDB balloon on 17 May 2016.

4 Discussion and Conclusions

Here we have presented evidence that lightning infrasound was observable by acoustic instruments suspended at stratospheric altitudes by free-flying balloons. Several waveforms were matched with detected lightning strokes through a simple time delay approach (Fig. 4c, d, e). Our matches are supported by a positive linear relationship between the WWLLN energy estimation for the matched lightning strokes and the energy densities calculated from the acoustic waveforms (Fig. S4 in supplementary info). Here, we have assumed that the signals represent direct arrivals between the source and receiver. To test this assumption, we searched for eigenray solutions using the GeoAc software package. Direct arrivals for all three waveforms are found for the distances and azimuths to their associated lightning strokes (Fig. S5 in supplementary info). However, the arrival times calculated using the eigenray paths described earlier do not readily match with the recorded arrival times of signals (Fig. S4 in supplementary information). It is worth noting that there were a number of signals recorded that do not readily match with any lightning strokes detected by the WWLLN, and *vice versa* (Fig. 4a, b and Fig. S3 in supplementary info). If the estimated detection rates of the WWLLN are correct [11-30%; *Hutchins et al.*, 2012], then there may have been as many as 100-300 lightning strokes within 100 km of the ULDB. This number of high-amplitude signals was not recorded at the ULDB (Fig. 4b), therefore the total number signals recorded at the ULDB underrepresents the true total of lightning strokes that occurred within range of the balloon. This is similar to detection rates of lightning infrasound by ground-based instruments [e.g. *Farges and Blanc*, 2010]. Complex atmospheric conditions in thunderclouds likely refract the generated acoustic waves away from the receiver [*Jones and Bedard*, 2015]. Additionally, it is possible that not all lightning strokes generate measurable infrasound. This may be attributed to very low signal-to-noise ratios, especially for smaller lightning strokes or those located further from the instrument than the rest of the thun-

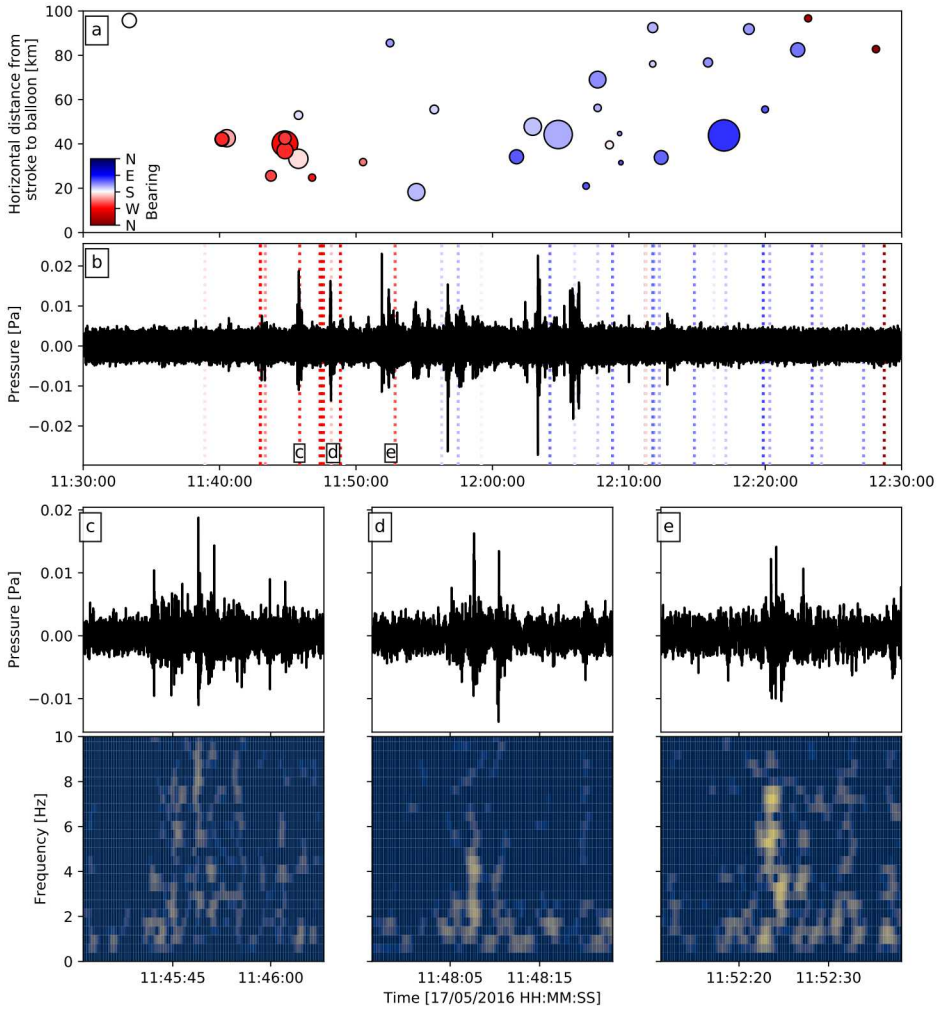

Figure 4. (a) Horizontal distances for each stroke within 100 km of the balloon from 1130 to 1230 UTC on 17 May 2016. each stroke is sized by the stroke energy, and colored by the bearing from the balloon to the stroke location. (b) High-pass (0.6 Hz) filtered acoustic waveform as recorded at the ULDB over the same time period. Vertical dotted lines indicate calculated time of arrivals for strokes in panel (a), colored by the bearing. Letters on bottom indicate locations of plotted example waveforms in panels c, d and e. (c,d,e) Example acoustic signals (top) from lightning strokes and their respective spectrograms (below).

derstorm cloud [*Farges and Blanc*, 2010]. This latter process is illustrated by a higher number of signals matches occurring during the storm approach towards the ULDB instead of during their divergence (Fig. 4b). A relatively low-frequency signal is recorded during an earlier storm at 0945 UTC (Fig. S3 in supplementary info). The low-frequency characteristic of this signal suggests an alternative source to lightning [e.g. meteors, transient luminous events; *Farges and Blanc*, 2010; *Edwards*, 2010], or that the original lightning signal was altered by absorption and/or directivity between the source and receiver.

For the ray propagation and eigenray modeling we have assumed a point source for the lightning infrasound at 4 km altitude. Infrasound sources from lightning have been

mapped up to 12 km altitude in the thundercloud [*Anderson et al.*, 2014; *Arechiga et al.*, 2014]. Furthermore, the mapped current flow within lightning strokes suggests the source geometry can resemble complex, dendritic structures [*Anderson et al.*, 2014]. To test whether our source shape and height assumption was viable, we have repeated the ray tracing modeling but with a source at 32 km height instead, the ULDB flying altitude. In reverse, this can be seen as all possible locations for sources whose acoustic waveforms will be recorded at the receiver. Results suggest that a receiver at 32 km should record signals from heights up to 12 km and take-off angles between 45-90° within a 100 km horizontal range in all directions (Fig. S6 in supplementary information). Therefore, the source configuration used for the raypath modeling was reasonable for the lightning infrasound described here.

A key assumption here was that the atmospheric conditions during the generation of the lightning infrasound was relatively simple and stratified. Thunderstorms require unstable air to form and persist, and often include significant vertical wind shear due to thermal plumes. The wind and temperature profiles used for ray path modeling here was likely a highly simplified representation of reality. Ray tracing from sources directly below thermal plumes such as those found within thunderstorm clouds have shown how they may act as vertical waveguides and thus can greatly distort the acoustic wavefield [*Jones and Bedard*, 2015]. Ray paths are found to either converge or diverge at the top of the thermal plume dependent on the height and width of the plume [*Jones and Bedard*, 2015]. Therefore the ray-paths and eigenrays presented here are likely an oversimplified representation of the true paths taken by the acoustic waves before their detection at the ULDB. Future studies of acoustic wavefields generated by lightning infrasound must take into account the complex refraction patterns induced by vertical columns of wind shear within thunderclouds.

The measured waveforms do not display the compression-rarefaction-compression shape that had been modeled as generated by a rapid intensification and discharge of the electric field in the thundercloud [*Pasko*, 2009]. It must be noted that the waveforms modeled by *Pasko* [2009] are of 0.1-1 Hz frequency and the acoustic wavefield was strongly oriented in the vertical direction [*Dessler*, 1973]. The detection of lightning infrasound from strokes at more than several tens of kilometers from the ULDB does not support the theory that acoustic wavefields generated by lightning infrasound are strictly oriented vertically. Instead, the waveforms here share amplitude, frequency and range detection characteristics with previously recorded lightning infrasound signals which were attributed to charge deposition in the lightning channels [e.g. *Farges and Blanc*, 2010; *Arechiga et al.*, 2014]. The electrostatic forces caused by the charge deposition may cause the air in the streamer zone to expand, producing an acoustic compression wave whose period corresponds to the size of the streamer zone [*Arechiga et al.*, 2014].This is in addition to the rapid air expansion generated by extreme heating of the lightning channel that produces audible and infrasonic acoustic waves [*Few et al.*, 1967].

The observations here of lightning infrasound recorded by a high-altitude balloon over the Tasman Sea in May 2016 are fortuitous. Yet,they also demonstrate the potential for using these platforms to expand our understanding of how infrasound may be generated by lightning strokes. While the observations presented here support the charge deposition mechanism postulated by *Arechiga et al.* [2014], we cannot yet rule out other possible mechanisms. Previous studies of these processes have thus far used only ground-based instruments which only offer an approximately two-dimensional view of the acoustic wavefield. Future studies which incorporate both balloon- and ground-based instruments will have an opportunity to capture a three-dimensional view of the infrasonic waves generated during lightning storms. Furthermore, simultaneous deployments of multiple instrument-bearing balloons are able to calculate back-azimuths to each infrasound source [e.g. *Bowman and Albert*, 2018], as well as provide the elevation angle of incoming sources [see Supplemental information in *Bowman and Lees*, 2018]. The lightning infrasound sig-

nals presented here are derived from strokes occurring >100 km from any significant landmass where ground-based instruments would be located, meaning these signals may never have been recorded otherwise. Therefore, balloon-based instruments offer a way to record signals from events which may not otherwise have been recorded by established infrasound instrument networks. As well as oceanic thunderstorms, this may include Transient Luminous Events [e.g. sprites; *Farges and Blanc*, 2010], meteors [e.g. *Edwards*, 2010], and supersonic auroral arcs [e.g. *Pasko*, 2012].

Acknowledgments

We would like to thank the NASA Balloon Program Office and the NASA Columbia Scientific Ballooning Facility for hosting our instrumentation on the 2016 Ultra Long Duration Balloon Mission. The authors also wish to thank the World Wide Lightning Location Network (http://wwlln.net), a collaboration including over 50 institutions, for providing the lightning data used in this paper. The acoustic data presented here is accessible at datadryad.org under the following doi: 10.5061/dryad.40877s4. This work was supported by National Science Foundation Grant AGS-1551999. Sandia National Laboratories is a multi-mission laboratory managed and operated by National Technology and Engineering Solutions of Sandia, LLC., a wholly owned subsidiary of Honeywell International, Inc., for the U.S. Department of Energy's National Nuclear Security Administration under contract DE-NA0003525. The views expressed here do not necessarily reflect the views of the United States Government, the United States Department of Energy, or Sandia National Laboratories. We would like to thank Jelle Assink and the anonymous reviewers whose comments and suggestions helped improve this manuscript.

References

Anderson, J. F., J. B. Johnson, R. O. Arechiga, and R. J. Thomas (2014), Mapping thunder sources by inverting acoustic and electromagnetic observations, *Journal of Geophysical Research: Atmospheres*, *119*(23), 13,287–13,304, doi:10.1002/2014JD021624.

Anderson, W. J., and I. Taback (1991), Oscillation of High-Altitude Balloons, *Journal of Aircraft*, *28*(9), 606–608.

Arechiga, R., M. Stock, R. Thomas, H. Erives, W. Rison, H. Edens, and J. Lapierre (2014), Location and analysis of acoustic infrasound pulses in lightning, *Geophysical Research Letters*, *41*(13), 4735–4744, doi:10.1002/2014GL060375.

Assink, J. D., L. G. Evers, I. Holleman, and H. Paulssen (2008), Characterization of infrasound from lightning, *Geophysical Research Letters*, *35*(15), 1–5, doi:10.1029/2008GL034193.

Balachandran, N. K. (1983), Acoustic and electric signals from lightning, *Journal of Geophysical Research: Oceans*, *88*(C6), 3879–3884, doi:10.1029/JC088iC06p03879.

Behnke, S. A., and S. R. McNutt (2014), Using lightning observations as a volcanic eruption monitoring tool, *Bulletin of Volcanology*, *76*(847), doi:10.1007/s00445-014-0847-1.

Blackstock, D. (2000), *Fundamentals of Physical Acoustics*, John Wiley and Sons.

Blanc, E., A. Le Pichon, L. Ceranna, T. Farges, J. Marty, and P. Herry (2010), Global Scale Monitoring of Acoustic and Gravity Waves for the Study of the Atmospheric Dynamics, in *Infrasound Monitoring for Atmospheric Studies*, edited by A. Le Pichon, E. Blanc, and A. Hauchecorne, pp. 647–664, Springer Netherlands, Dordrecht.

Blom, P., and R. Waxler (2012), Impulse propagation in the nocturnal boundary layer: Analysis of the geometric component, *The Journal of the Acoustical Society of America*, *131*(5), 3680–3690, doi:10.1121/1.3699174.

Bohannon, J. L., A. A. Few, and A. J. Dessler (1977), Detection of Infrasonic Pulses from Thunderclouds, *Geophysical Research Letters*, *4*(2), 49–52.

Bowman, D. C., and S. A. Albert (2018), Acoustic Event Location and Background Noise Characterization on a Free Flying Infrasound Sensor Network in the Stratosphere, *Geophysical Journal International*, *213*, 1524–1535, doi:10.1093/gji/ggy069.

Bowman, D. C., and J. M. Lees (2015), Infrasound in the middle stratosphere measured with a free-flying acoustic array, *Geophysical Research Letters*, *42*(22), 10,010–10,017, doi:10.1002/2015GL066570.

Bowman, D. C., and J. M. Lees (2017), A Comparison of the Ocean Microbarom Recorded on the Ground and in the Stratosphere, *Journal of Geophysical Research: Atmospheres*, *122*(18), 9773–9782, doi:10.1002/2017JD026474.

Bowman, D. C., and J. M. Lees (2018), Upper atmosphere heating from ocean-generated acoustic wave energy, *Geophysical Research Letters*, doi:10.1029/2018GL077737.

Bowman, D. C., J. M. Lees, J. A. Cutts, E. F. Young, K. T. Seiffert, M. Boslough, and S. J. Arrowsmith (2017), Geoacoustic Observations on Drifting Balloon-Borne Sensors, in *Infrasound Monitoring for Atmospheric Studies*, edited by A. Le Pichon, E. Blanc, and A. Hauchecorne, 2 ed.

Campus, P., and D. Christie (2010), Worldwide Observations of Infrasonic Waves, in *Infrasound Monitoring for Atmospheric Studies*, edited by A. Le Pichon, E. Blanc, and A. Hauchecorne, pp. 185–234, Springer Netherlands.

Christie, D. R., and P. Campus (2010), The IMS Infrasound Network: Design and Establishment of Infrasound Stations, in *Infrasound Monitoring for Atmospheric Studies*, edited by A. Le Pichon, E. Blanc, and A. Hauchecorne, pp. 29–75, Springer Netherlands.

Dessler, A. J. (1973), Infrasonic thunder, *J. Geophys. Res.*, *78*(12), 1889–1896, doi:10.1029/JC078i012p01889.

Dowden, R. L., R. H. Holzworth, C. J. Rodger, J. Lichtenberger, N. R. Thomson, A. R. Jacobson, E. Lay, J. B. Brundell, T. J. Lyons, S. O'Keefe, Z. Kawasaki, C. Price, V. Prior, P. Ortéga, J. Weinman, Y. Mikhailov, O. Veliz, X. Qie, G. Burns, A. Collier, O. Pinto Junior, R. Diaz, C. Adamo, E. R. Williams, S. Kumar, G. B. Raga, J. M. Rosado, E. E. Avila, M. E. Clilvera, T. Ulich, P. Gorham, T. J. G. Shanahan, T. Osipowicz, G. Cook, and Y. Zhao (2008), World-Wide Lightning Location Using VLF Propagation in the Earth-Ionosphere Waveguide, *IEEE Antennas and Propagation Magazine*, *50*(5), 40–60.

Edwards, W. N. (2010), Meteor Generated Infrasound: Theory and Observation, in *Infrasound Monitoring for Atmospheric Studies*, edited by A. Le Pichon, E. Blanc, and A. Hauchecorne, pp. 361–414, Springer Netherlands, Dordrecht, doi:10.1007/978-1-4020-9508-5_12.

Farges, T., and E. Blanc (2010), Characteristics of infrasound from lightning and sprites near thunderstorm areas, *Journal of Geophysical Research: Space Physics*, *115*(A6), doi:10.1029/2009JA014700.

Fee, D., and R. S. Matoza (2013), An overview of volcano infrasound: From hawaiian to plinian, local to global, *Journal of Volcanology and Geothermal Research*, *249*, 123–139, doi:10.1016/j.jvolgeores.2012.09.002.

Few, A., A. Dessler, D. Latham, and M. Brook (1967), A dominant 200-hertz peak in the acoustic spectrum of thunder, *Journal of Geophysical Research*, *72*(24), 6149–6154.

Few, A. A. (1969), Power Spectrum of Thunder Divergence, *Journal of Geophysical Research*, *74*(28), 6926–6934, doi:10.1029/JC074i028p06926.

Hutchins, M. L., R. H. Holzworth, C. J. Rodger, and J. B. Brundell (2012), Far-Field power of lightning strokes as measured by the world wide lightning location network, *Journal of Atmospheric and Oceanic Technology*, *29*(8), 1102–1110, doi:10.1175/JTECH-D-11-00174.1.

Jones, R. M., and A. J. Bedard (2015), Infrasonic ray tracing applied to small-scale atmospheric structures: Thermal plumes and updrafts/downdrafts, *The Journal of the Acoustical Society of America*, *137*(2), 625–632, doi:10.1121/1.4906175.

Kim, K., and J. M. Lees (2014), Local Volcano Infrasound and Source Localization Investigated by 3D Simulation, *Seismological Research Letters*, *85*(6), 1177–1186, doi:10.1785/0220140029.

Lacanna, G., and M. Ripepe (2013), Influence of near-source volcano topography on the acoustic wavefield and implication for source modeling, *Journal of Volcanology and Geothermal Research*, *250*, 9–18, doi:10.1016/j.jvolgeores.2012.10.005.

Marcillo, O., J. B. Johnson, and D. Hart (2012), Implementation, characterization, and evaluation of an inexpensive low-power low-noise infrasound sensor based on a micromachined differential pressure transducer and a mechanical filter, *Journal of Atmospheric and Oceanic Technology*, *29*(9), 1275–1284, doi:10.1175/JTECH-D-11-00101.1.

Pasko, V. P. (2009), Mechanism of lightning-associated infrasonic pulses from thunderclouds, *Journal of Geophysical Research Atmospheres*, *114*(8), 1–10, doi:10.1029/2008JD011145.

Pasko, V. P. (2012), Infrasonic waves generated by supersonic auroral arcs, *Geophysical Research Letters*, *39*(19), 1–5, doi:10.1029/2012GL053587.

Supporting Information for
"Detecting lightning infrasound using a high-altitude balloon"

Oliver D. Lamb[1], Jonathan M. Lees[1], Daniel C. Bowman[2]

[1]Department of Geological Sciences, The University of North Carolina at Chapel Hill, Chapel Hill, North Carolina, USA

[2]Sandia National Laboratories, Albuquerque, New Mexico, USA

Contents

1. Figures S1 to S6

Additional Supporting Information (Files uploaded separately)

1. Caption for Movie S1

Introduction

Supplementary information provides Figures S1 to S6, and a caption for Movie S1.

Movie S1.

Animated version of Figure 1 in the main article. Each frame covers a 10 min interval as the ULDB (Red Triangle) flies over the Tasman Sea from 0600 to 1800 UTC on 17 May 2016. Locations of lightning strokes detected by the WWLLN are also plotted, and coloured by age for up to an hour.

Corresponding author: Oliver Lamb, olamb@email.unc.edu

Figures S1 to S6

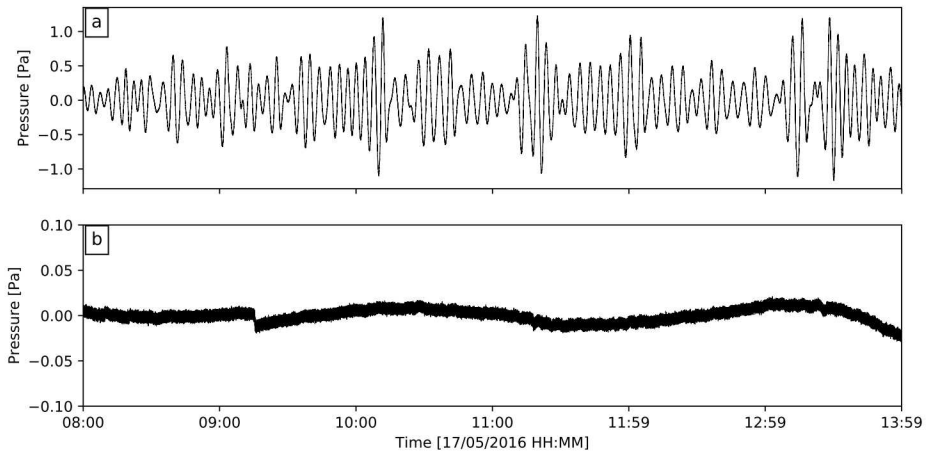

Figure S1 : Unfiltered acoustic waves as recorded by the acoustic package on the ULDB. (a) The combined acoustic wave as recorded by the reversed polarity pair of instruments. (b) 'Acoustic' waveform as recorded by the disabled 'control' instrument in the acoustic package. The source of the jump at 0915 UTC is unknown but has no apparent effect on the acoustics recorded by the reversed polarity pair.

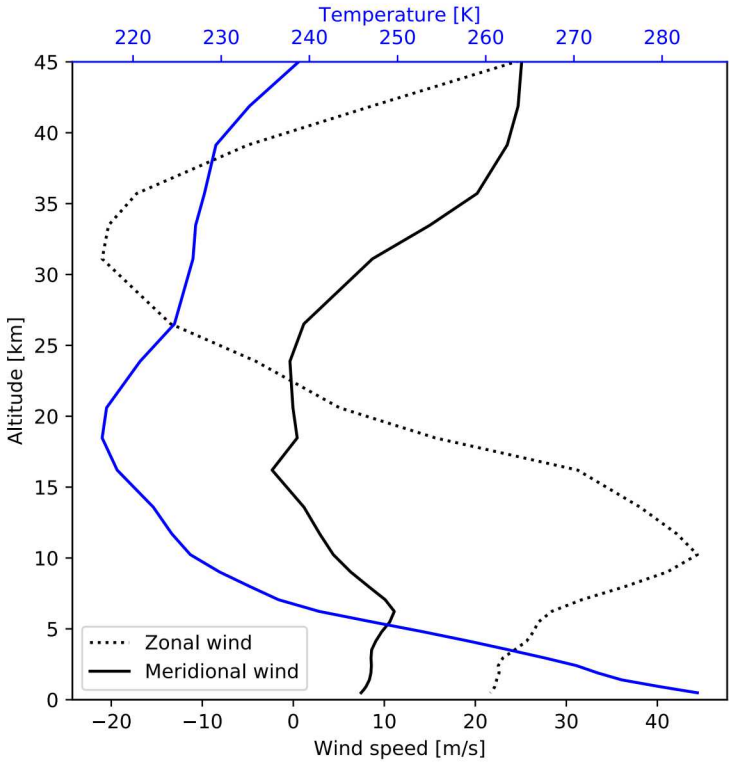

Figure S2 : Atmospheric profile above the Tasman Sea used for ray path propagation modeling, derived from the Global Forecast System model from NOMADS at 12z on 17 May 2016.

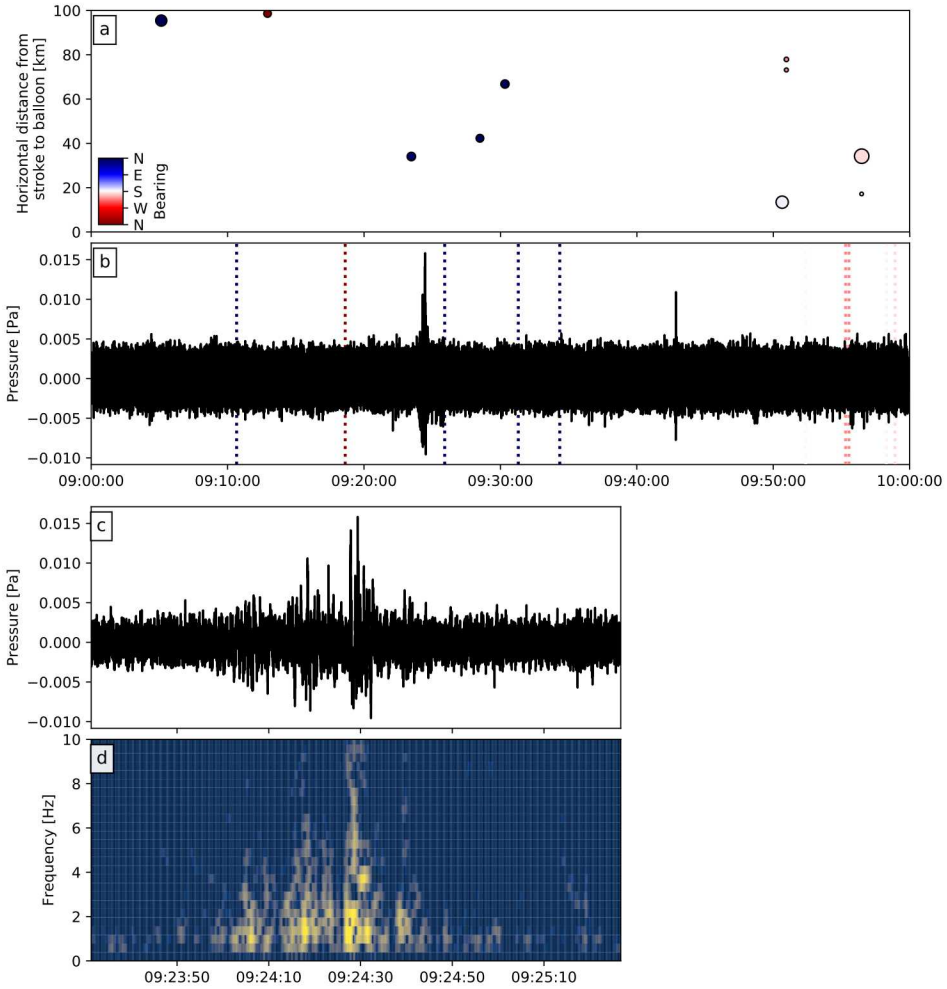

Figure S3 : (a) Horizontal distances for each stroke within 100 km of the balloon from 0900 to 1000 UTC on 17 May 2016. each stroke is sized by the stroke energy, and colored by the bearing from the balloon to the stroke location. (b) High-pass filtered acoustic waveform as recorded at the ULDB over the same time period. Vertical dotted lines indicate calculated time of arrivals for strokes in panel (a), colored by the bearing. (c) Possible example acoustic signal from lightning stroke and its frequency spectrogram (d).

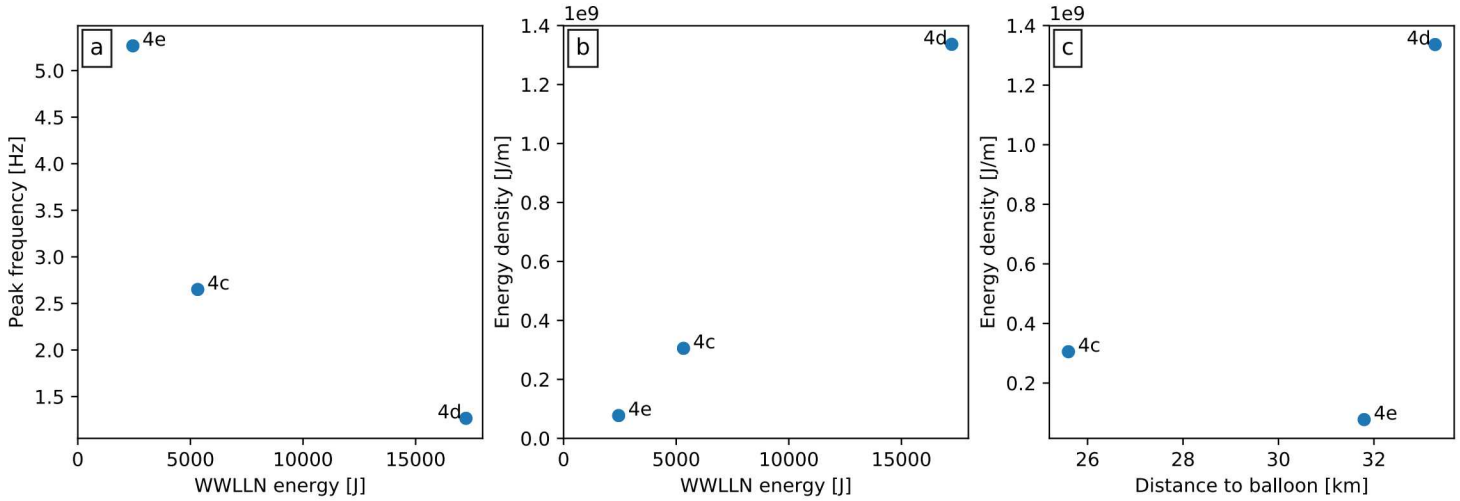

Figure S4 : Results of calculating the energy density of the lightning strokes from the acoustic waves plotted in Fig 4c, d, and e. (a) Calculated peak frequency of each wave plotted against the detected energy by the WWLLN for matching lightning strokes. (b) Calculating energy densities for each waveform versus the detected energy by the WWLLN for matching lightning strokes. (c) Calculated energy densities for each waveform versus the distance between the matching lightning stroke and balloon.

Confidential manuscript submitted to *Geophysical Research Letters*

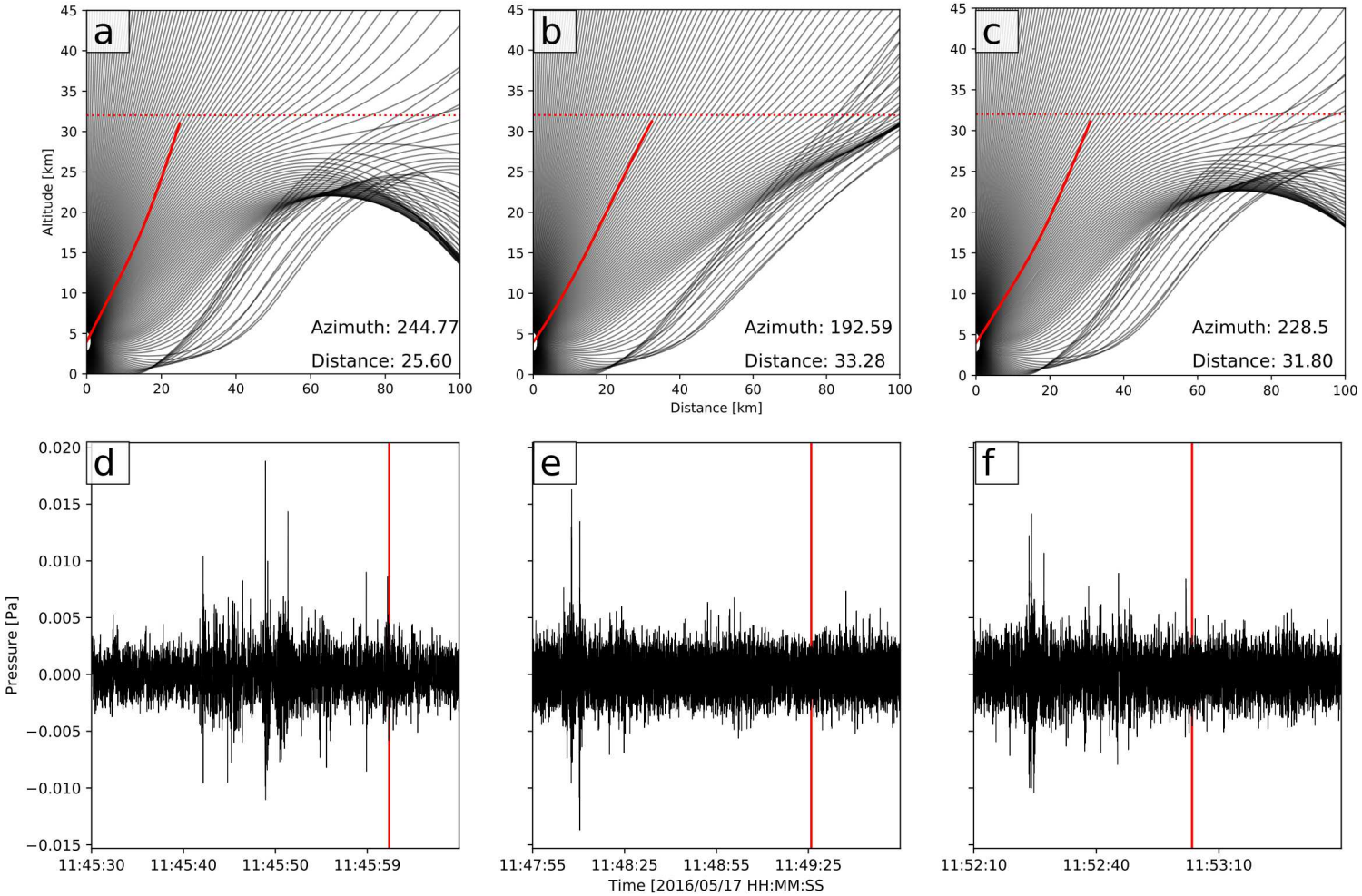

Figure S5 : Ray path propagation results (black lines) and eigenray solutions between a source and the receiver at the ULDB, for signals detailed in Figure 4c, d, and e (a, b and c, respectively). Azimuth and horizontal distances between source and receivers are detailed within each panel. Panels d, e, and f plot the waveforms with calculated arrival times from the eigenray solutions (red lines).

Confidential manuscript submitted to *Geophysical Research Letters*

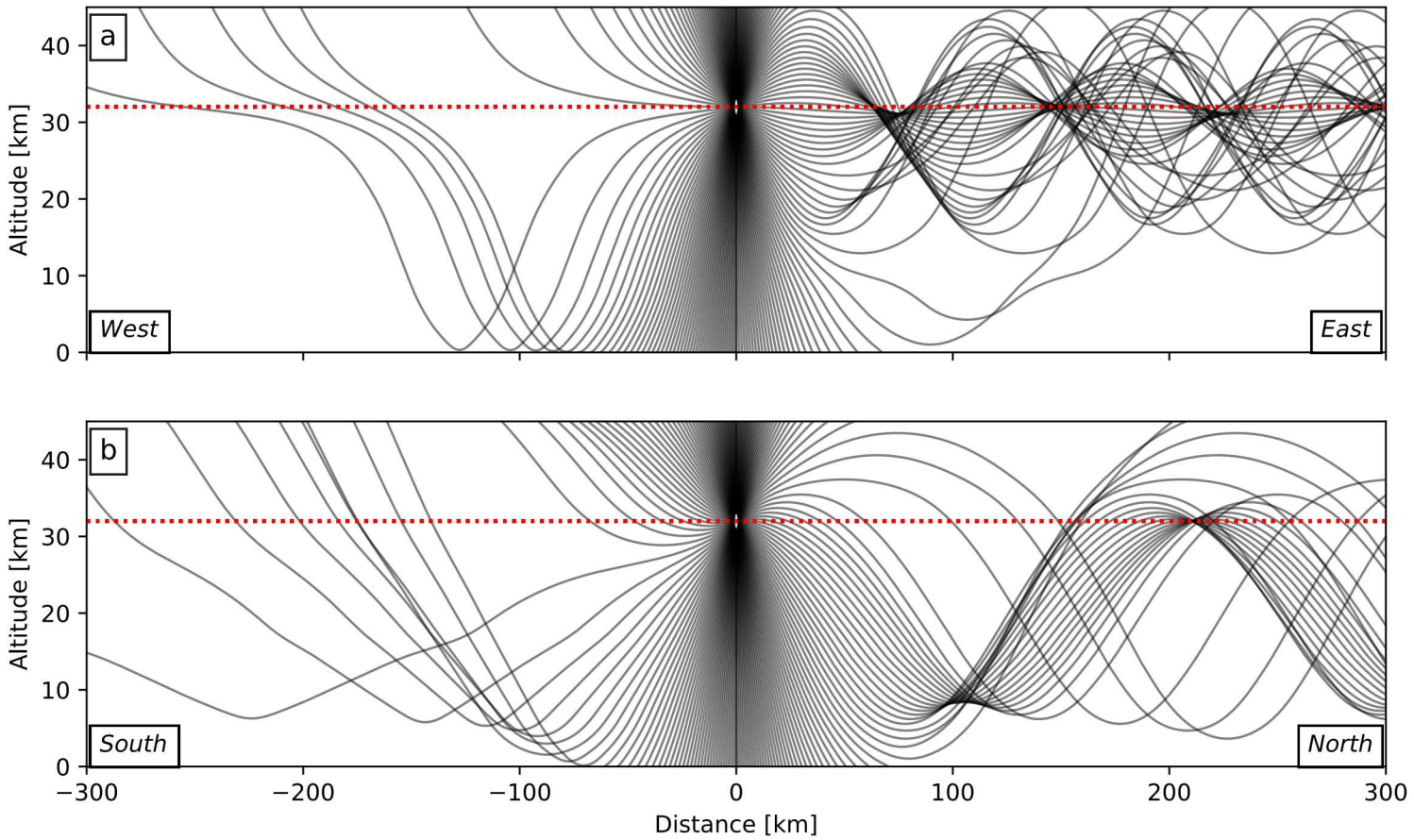

Figure S6 : Ray-tracing propagation for an acoustic source at 32 km height along East-West (a) and North-South (b) profiles using realistic atmospheric conditions derived from the Global Forecast System. The red dotted line at 32 km indicates the average height of the ULDB balloon on 17 May 2016.

Confidential manuscript submitted to *Geophysical Research Letters*